Wind and Structures, *Vol. 16, No. 5 (2013) 517-540*
DOI:http://dx.doi.org/10.12989/was.2013.16.5.517

Understanding of unsteady pressure fields on prisms based on covariance and spectral proper orthogonal decompositions

Le Thai Hoa*[1,2], Yukio Tamura[3], Masaru Matsumoto[4] and Hiromichi Shirato[4]

[1]Wind Engineering Research Center, Tokyo Polytechnic University,1583 Iiyama, Atsugi, Kanagawa 243-0297, Japan
[2]Hanoi University of Engineering and Technology, Vietnam National University, Hanoi,144 Xuan Thuy, Cau Giay, Hanoi, Vietnam
[3]Department of Architectural Engineering, Tokyo Polytechnic University,1583 Iiyama, Atsugi, Kanagawa 243-0297, Japan
[4]Department of Civil Engineering, Kyoto University, Kyoto-Daigaku-Katsura, Nishikyo, Kyoto 615-8530, Japan

(Received September 3, 2011, Revised May 18, 2012, Accepted May 23, 2012)

Abstract. This paper presents applications of proper orthogonal decomposition in both the time and frequency domains based on both cross spectral matrix and covariance matrix branches to analyze multi-variate unsteady pressure fields on prisms and to study spanwise and chordwise pressure distribution. Furthermore, modification of proper orthogonal decomposition is applied to a rectangular spanwise coherence matrix in order to investigate the spanwise correlation and coherence of the unsteady pressure fields. The unsteady pressure fields have been directly measured in wind tunnel tests on some typical prisms with slenderness ratios B/D=1, B/D=1 with a splitter plate in the wake, and B/D=5. Significance and contribution of the first covariance mode associated with the first principal coordinates as well as those of the first spectral eigenvalue and associated spectral mode are clarified by synthesis of the unsteady pressure fields and identification of intrinsic events inside the unsteady pressure fields. Spanwise coherence of the unsteady pressure fields has been mapped the first time ever for better understanding of their intrinsic characteristics.

Keywords: unsteady pressure; pressure distribution; spanwise correlation; spanwise coherence; coherence mapping; covariance proper orthogonal decomposition; spectral proper orthogonal decomposition

1. Introduction

Aerodynamic phenomena on a structure immersed in atmospheric turbulent flows are generated by a spatial distribution and a correlation of unsteady pressure fields on a surface of structural section. In particular, the spatial distribution and correlation are key issues for estimating turbulence-induced buffeting forces and buffeting responses of the structure in the turbulent flows. The unsteady pressure field is generally considered as a spatially-correlated multi-variate random Gaussian one. For typical cases of prisms and bridge deck sections, understanding of chordwise

*Corresponding author, Professor, E-mail: thle@vnu.edu.vn

http://www.techno-press.org/?journal=was&subpage=8 ISSN: 1226-6116 (Print), 1598-6225 (Online)

distribution and spanwise correlation of the unsteady pressure field makes it possible to reveal and interpret mechanisms of excitations, and to identify the responses of aerodynamic phenomena on these structures. Due to the nature of a multi-variate random field, however, the unsteady pressure field is considered as a superposition from some causes and excitations of dominant physical phenomena. It is logical to decompose the unsteady pressure field by sums of independent partial pressure fields, which can be related to a particular mechanism of excitation and certain physical phenomena.

Proper orthogonal decomposition (POD), also known as Karhunen-Loeve decomposition or principal component analysis (PCA), was developed by Loeve 1945 and Karhunen 1946 and was first applied to analysis of multi-variate turbulent fields by Lumley 1970, Berkooz *et al*. 1993. Originally, POD was a purely mathematical tool for linear transformation of spatially-correlated multi-variate random Gaussian fields into time-dependant uncorrelated uni-variate sub-processes (also called principal components or principal coordinates) and basic orthogonal vectors (space functions or POD modes) using eigenvalue decomposition or spectral decomposition. Pairs of principal coordinate and POD mode, especially the lowest-order pairs, can be thought of as revealing the internal structure, intrinsic event and physical interpretation of these random fields.

This is because: (i) Pairs are independent and orthogonal and (ii) Low-order pairs are strongly contributive from fast-decaying spectral decomposition. Although POD originally involves eigenvalue decomposition of positive-definite real square matrices, in the broad sense it can deal with different types of matrices thanks to decomposition techniques, i.e., using Schur decomposition for complex square matrices or singular value decomposition for both real and complex rectangular matrices. Relationships between decomposition techniques and modification of POD can be referred elsewhere (e.g.., Liang *et al*. 2002, Solari *et al*. 2007). Due to its advantages, POD also has been widely used in many engineering fields such as analysis and synthesis, reduced-order modeling, simulation of multi-variate random fields, numerical analysis, system identification, stochastic response and so on (Liang *et al*. 2002). In the wind engineering, POD has been applied to several main topics such as: (i) Analysis and synthesis of the multi-variate random fields including turbulent fields, unsteady pressure fields and turbulence-induced force fields, (ii) Representation and simulation of the multi-variate random turbulent fields and (iii) Stochastic responses of structures (e.g., Solari *et al*. 2007, Carassale *et al*., 2007). POD has been commonly branched into either covariance matrix-based or cross spectral matrix-based proper orthogonal decompositions, which depend on how to build up a basic matrix from either zero-time-lag covariance or cross spectral matrices of multi-variate random fields. However, it can be extended to rectangular matrices depending on the purpose of the study to deal with such data matrix, correlation matrix or coherence matrix of the multi-variate random fields.

A lot of literatures have applied POD to analysis and synthesis of spatially-correlated multi-variate pressure fields on prisms and structures. However, most applications in the covariance POD branch use the covariance matrix of unsteady pressure fields due to its straightforward computation and interpretation. It is rarely used for unsteady pressure fields. Some authors have used the covariance POD to analyze experimental unsteady pressure fields and to determine the relation between the covariance POD modes and the physical phenomena on the models. Bienkiewicz *et al*. 1995, used the POD analysis of mean and fluctuating pressure fields around a low-rise building in turbulent flows. A linkage between the pattern of the pressure distribution and POD modes, especially the first two covariance POD modes, has been discussed and interpreted, in which the 1st mode was compatible with the pattern of the fluctuating pressure distribution, whereas the 2nd mode was similar to the mean pressure pattern. The effect of pressure tap positions on the same measured pressure area (uniform and non-uniform arrangements) on the covariance POD modes was investigated by Jeong *et al*. 2000, by which the covariance POD mode observations were different in two cases. Kikuchi et al. 1997 applied an unsteady pressure field to tall buildings, and the fluctuating pressure field was reconstructed for only a few dominant POD modes, and was used to estimate aerodynamic forces and corresponding responses. Tamura *et al*. 1999 indicated distortion and wrong interpretation of the POD modes due to the presence of mean pressure data in the analyzed pressure field. It is shown that POD is a powerful tool for revealing physical phenomena from experimental data. Correspondence between the covariance POD modes and the physical causes of the fluctuating pressure field has been observed in many cases.

However, some others have argued that interpretation from the covariance POD modes is aprioristic and arbitrary based on previous knowledge of field behavior and response. Holmes *et al*. 1997, showed that there were no consistent linkages between the physical phenomena and the POD mode thanks to a series of physical measurements and covariance POD analyses of the pressure fields on low-rise buildings. Some reasons for this misleading are: (i) POD relies on the linear transformation tool with constraint and sensitiveness to orthogonal conditions, (ii) Representation of the pressure field via the covariance matrix is not convincing and frequency-dependant factors occurring in physical systems cannot be updated, and (iii) Physical interaction is not always clearly decoupled by separate and independent events. It is also argued that the contribution and importance of the lowest-order POD modes might depend on many factors such as number of pressure taps, pressure arrangement, mean value presence, model geometry, complexities of turbulence and bluff body flows and so on. Accuracy of physical interpretation of the lowest-order POD modes accordingly reduces with decrease in the contribution of the lowest-order POD modes. Application of the spectral POD in the frequency domain to the unsteady pressure fields is none due to difficulty in computation and result interpretation, but solely De Grenet and Ricciardelli 2004, recently tried applying the spectral POD to the study of an unsteady pressure field on a square prism and a bridge deck.

Spatial correlation of the pressure fields or buffeting forces can be expressed either by the correlation coefficient function in the time domain or by the coherence function in the frequency domain. For simplicity, however, the spatial distribution of the fluctuating velocity field (or turbulence fields) has been used to replace for the turbulence-induced pressures and forces. It is also assumed, moreover, that the spanwise coherence of the turbulence-induced forces is similar to that of the ongoing turbulence that was simplified as an exponential coherence formula used so far for predicting the buffeting response of a structure (Davenport 1963). Recent literatures, however, show that the coherence of turbulence-induced pressures and forces was larger than that of the ongoing turbulence (Larose 1996, Jakobsen 1997, Kimura *et al*. 1997, Matsumoto *et al*. 2003).

They argued that the influence of a structure on ongoing turbulent flows must not be negligible, and interaction phenomena between them and the structure might be the cause of a modification of ongoing turbulent flows around the structure (one is mentioned as bluff body flow). Uncertainty of the coherence of turbulence-induced pressures and forces higher than that of turbulence can cause underestimation of the buffeting response of a structure. The mechanism of this higher coherence, coherent structures of turbulence and pressure as well as effect of the bluff body flow on coherence must be further clarified to reduce analytical risks. So far, the Fourier transform-based correlation function and the coherence one have been used to study the spanwise correlation and spanwise coherence of unsteady pressure fields. Spanwise correlations and coherences of turbulence and pressure have been presented by several authors (e.g., Kareem 1997). Covariance POD modes for studying the cross correlation of an unsteady pressure field was first used in Tamura *et al*. 1997.

Recently, POD-based and the wavelet transform-based tools have been applied to investigate spanwise correlation, spanwise coherence and coherent structures of turbulence and pressure fields (Kareem and Kijewski 2002, Le *et al*. 2009). The effects of spanwise separations, bluff body flow, and ongoing flow conditions on the coherence of turbulence and pressure, as well as intermittent distribution of the coherence and tempo-spectral correspondence between the coherence of turbulence and of pressure in the time-frequency plane have been investigated (Le *et al*. 2009). Spectral POD has been extended for mapping the coherence of unsteady pressure fields (Le *et al*. 2011) in which the effects of spanwise separations and bluff body flow are apparently observed through these coherence maps.

This paper presents applications of both covariance and spectral POD branches to experimental unsteady pressure fields on some typical prisms. Furthermore, POD is extended to investigate the spanwise coherence of these unsteady pressure fields. The importance of the lowest-order covariance POD modes and spectral POD modes are discussed and compared, and possible relationships between the POD modes and the physical phenomena relating to characteristics of the bluff body flows are classified for better understanding. Unsteady pressure fields have been experimentally measured on some typical prisms with slenderness ratios of B/D=1, B/D=1 with splitter plate and B/D=5 in a wind tunnel.

2. Proper orthogonal decomposition

2.1 Definition

POD provides an optimum approximation of multi-variate random fields, comprising the unsteady pressure field. The main idea of POD is to obtain a set of orthogonal basic vectors that can expand the multi-variate random field into a sum of products of these basic orthogonal vectors (or modes) and uni-variate uncorrelated random processes. The unsteady pressure field is expressed as

$$P(\upsilon,t) = \overline{p}(\upsilon) + p(\upsilon,t) \tag{1}$$

where $P(\upsilon,t)$: unsteady pressure; $\overline{p}(\upsilon)$: mean pressure; $p(\upsilon,t)$: fluctuating pressure; υ: spatial variables (υ=x;y;z).

Fluctuating pressure field $p(\upsilon,t)$ is usually represented as an N-variate Gaussian random process with zero mean containing sub-processes at N points in the field: $p(\upsilon,t) = \{p_1(\upsilon,t), p_2(\upsilon,t),..., p_N(\upsilon,t)\}$.

The fluctuating pressure field can be expressed as the following approximation

$$p(\upsilon,t) = a(t)^T \Phi(\upsilon) \approx \sum_{i}^{\tilde{N}} a_i(t)\phi_i(\upsilon) \tag{2}$$

where $a(t), \Phi(\upsilon)$: principal coordinates and space function $a(t) = \{a_1(t), a_2(t),..., a_N(t)\}$, $\Phi(\upsilon) = [\phi_1(\upsilon), \phi_2(\upsilon),..., \phi_N(\upsilon)]$; $a_i(t)$: i-th principal coordinate as uni-variate zero-mean random processes $E[a_i(t)] = 0$; $\phi_i(\upsilon)$: i-th basic orthogonal vector $\phi_i(\upsilon)^T \phi_j(\upsilon) = \delta_{ij}$ (δ_{ij} : Kronecker delta); N: total number of pairs of the principal coordinates and the orthogonal vectors; and $\tilde{N}$: truncated number of pairs of principal coordinate and orthogonal vector for approximation.

A mathematical expression of optimality expresses the space function $\Phi(\upsilon)$ that maximizes the projection of the random field $p(\upsilon,t)$ onto this space function, suitably normalized on the mean square basis (Lumley 1970)

$$Max \left\lfloor \left\langle |\, (p(\upsilon,t) \otimes \Phi(\upsilon))\,|^2 \right\rangle \Big/ \left\|\Phi(\upsilon)\right\|^2 \right\rfloor \tag{3}$$

where $(\otimes), \langle . \rangle, |.|, \|.\|$ denote inner product, expectation, absolute and Euler squared norm operators, respectively..

2.2. Covariance proper orthogonal decomposition

The optimality in Eq.(3) can be expanded in the form of equality (Lumley 1970)

$$\int_{L_\upsilon} R_{p_i p_j}(\upsilon_i, \upsilon_j, t)\Phi(\upsilon_j)d\upsilon_j = \lambda\Phi(\upsilon) \tag{4}$$

where $R_{p_i p_j}(\upsilon_i, \upsilon_j, t)$: covariance value as a spatial correlation between two positions υ_i, υ_j in the pressure field; λ : weighted coefficient; and L_υ : space of the pressure field.

Thus, the solution of the space function $\Phi(\upsilon)$ can be determined as the eigen problem of the covariance matrix of the fluctuating pressure field as follows

$$R_p(\upsilon,t)\Phi(\upsilon) = \Lambda\Phi(\upsilon) \tag{5}$$

where $R_p(\upsilon,t)$: covariance matrix of fluctuating pressure field, which is defined as $R_p(\upsilon,t) = \left\lfloor R_{p_i p_j}(\upsilon,t) \right\rfloor_{NxN}$, where $R_{p_i p_j}(\upsilon,t) = E\left[p_i(\upsilon,t)^T p_j(\upsilon,t)\right]$; $p_i(\upsilon,t)$, $p_j(\upsilon,t)$: fluctuating pressure sub-processes at positions υ_i and υ_j; E: expectation operator; Λ : diagonal eigenvalue matrix $\Lambda = diag(\lambda_1, \lambda_2, ..., \lambda_N)$; and $\Phi(\upsilon)$: covariance space function, containing orthogonal vectors (also called covariance POD modes). It is noted that because the covariance matrix of the pressure field is real symmetric square and positive-definite, the eigenvalues are positive real and the covariance POD modes are real.

The multi-variate fluctuating pressure field can be approximated by using a limited number of low-order covariance POD modes

$$p(\upsilon,t) = a(t)\Phi(\upsilon) \approx \sum_{i=1}^{\tilde{N}} a_i(t)\phi_i(\upsilon) \tag{6}$$

In Eq. (6), the principal coordinates can be computed from measured data

$$a(t) = \Phi(\upsilon)^{-1} p_0(\upsilon,t) = \Phi(\upsilon)^T p_0(\upsilon,t) \tag{7}$$

where $p_0(\upsilon,t)$: measured data or observations.

In the covariance POD, some characteristics can be deducted from the eigen problem as follows

$$\Phi(\upsilon)^T \Phi(\upsilon) = I \text{ ; } \Phi(\upsilon)^T R_p(\upsilon,t)\Phi(\upsilon) = \Lambda \tag{8a}$$

$$E\left[a_i(t)^T a_j(t)\right] = \lambda_i \delta_{ij} \text{ ; } \sigma_{p_i}^2 = E\left[p_i(\upsilon,t)^2\right] = \lambda_i \text{ ; } R_{p_i p_j} \approx \sigma_{p_i}\sigma_{p_j}\sum_{k=1}^{\tilde{N}} \lambda_k \phi_{ik}\phi_{jk} \tag{8b}$$

where I: identity matrix; and σ_{p_i} : standard deviation of pressure sub-process $p_i(\upsilon,t)$.

The importance of pairs of eigenvalue and covariance POD mode to the pressure field can be quantitatively based on the concept of energy contribution. Accordingly, the contribution percentage of the i-th covariance POD mode on the total pressure field can be estimated based on either (i) proportion of eigenvalues or (ii) proportion of variance functions of the pressure field as follows

$$E_{\phi_i} = \lambda_i \Big/ \sum_{i=1}^{N} \lambda_i \text{ ; } E_{\phi_i} = \lambda_i \phi_i^2(\upsilon) \big/ \sigma_p^2 \tag{9}$$

where E_{ϕ_i} : energy contribution as a percentage of the i-th covariance POD mode ϕ_i ; λ_i : i-th eigenvalue; and σ_p : standard deviation of the pressure field.

Afterward, the covariance POD procedure is applied to analysis and synthesis of the experimental unsteady pressure fields on prisms.

2.3. Spectral proper orthogonal decomposition

Owing to the idea of the covariance POD and time domain-based formulations using the covariance matrix of the pressure field, the cross spectral matrix of the fluctuating pressure field is also exploited to formulate the spectral POD in the frequency domain. The cross spectral matrix of the pressure field can be defined as $S_p(\upsilon, f) = \left[S_{p_i p_j}(\upsilon, f)\right]_{NxN}$, $S_{p_i p_j}(\upsilon, f) = E\left[\hat{p}_i(\upsilon, f)^T \hat{p}_j(\upsilon, f)\right]$, where $\hat{p}_i(\upsilon, f)$, $\hat{p}_j(\upsilon, f)$: Fourier transforms of the fluctuating pressure sub-processes $p_i(\upsilon,t)$, $p_j(\upsilon,t)$ at spatial positions υ_i, υ_j ; and f: frequency variables.

Spectral space function $\Psi(\upsilon, f)$ depending on the frequency can be determined based upon the eigen problem of the cross spectral matrix $S_p(\upsilon, f)$ of the fluctuating pressure field $p(\upsilon,t)$

$$S_p(\upsilon, f)\Psi(\upsilon, f) = \Gamma(f)\Psi(\upsilon, f) \tag{10}$$

where $\Gamma(f), \Psi(\upsilon, f)$: spectral eigenvalues and spectral space function containing spectral eigenvectors (known also as spectral POD modes) orthogonalized at certain frequencies $\Gamma(f) = diag[\gamma_1(f), \gamma_2(f), ...\gamma_N(f)]$, $\Psi(\upsilon, f) = [\psi_1(\upsilon, f), \psi_2(\upsilon, f), ..., \psi_N(\upsilon, f)]$. Noting that the spectral eigenvalues are positive real or complex with a positive real part at each frequency and spectral POD modes are real or complex at certain frequencies due to the positive semi-definite symmetric square cross spectral matrix.

The fluctuating pressure field can be approximated using a limited number of low-order spectral POD modes as follows

$$\hat{p}(\upsilon, f) = \hat{a}(f)\Psi(\upsilon, f) \approx \sum_{i=1}^{\tilde{N}} \hat{a}_i(f)\psi_i(\upsilon, f) \quad , \tilde{N} < N \tag{11a}$$

$$S_p(\upsilon, f) = \Psi(\upsilon, f)\Gamma(f)\Psi\ (\upsilon, f)^{*T} \approx \sum_{i=1}^{\tilde{N}} \psi_i(\upsilon, f)\gamma_i(f)\psi_i\ (\upsilon, f)^{*T} \quad , \tilde{N} < N \tag{11b}$$

where $\hat{p}(\upsilon, f), \hat{S}_p(\upsilon, f)$: Fourier transform and power spectrum of reconstructed pressure field $p(\upsilon,t)$; *,T: complex conjugate and transpose operations; and $\hat{a}(f)$: spectral principal coordinates as Fourier transforms of uncorrelated uni-variate pressure sub-processes, which can be computed from measured data

$$\hat{a}(f) = \Psi(\upsilon, f)^{-1}\hat{p}_0(\upsilon, f) = \psi(\upsilon, f)^T \int_{-\infty}^{\infty} p_0(\upsilon,t)e^{i2\pi ft}dt \tag{12}$$

where $\hat{p}_0(\upsilon, f)$: Fourier transform of measured data or observations $p_0(\upsilon,t)$.

Some characteristics can be deducted from the spectral POD and the eigen problem as follows

$$\Psi^{*T}(\upsilon, f)\Psi\ (\upsilon, f) = I;\ \Psi^{*T}(\upsilon, f)S_p(\upsilon, f)\Psi\ (\upsilon, f) = \Gamma(f) \tag{13}$$

The energy contribution of the i-th spectral POD mode on total field energy can be determined as a proportion of spectral eigenvalues in a selected frequency range as follows

$$E_{\phi_i(f)} = \sum_{k=1}^{f_{cut-off}} \gamma_i(f_k) \Big/ \sum_{i=1}^{N} \sum_{k=1}^{f_{cut-off}} \gamma_i(f_k) \tag{14}$$

where $f_{cut-off}$: cut-off frequency in selected frequency range.

Let's also apply afore-mentioned spectral POD procedure to analysis and identification of the unsteady pressure fields on the experimental prisms.

2.4. Coherence matrix-based proper orthogonal decomposition

POD has used eigenvalue decomposition for square-formatted matrices like the covariance matrix and the cross spectral matrix of a multi-variate pressure field as above-mentioned. However, it can be extended to deal with rectangular-formatted matrices using singular value decomposition. POD aims here to decompose a spanwise coherence matrix of a multi-variate pressure field in order to extract intrinsic characteristics of the spanwise correlation in this pressure field. The spanwise coherence matrix can be defined as follows

$$COH_p(\Delta y, f) = \lfloor COH_{p_i p_j}(\Delta y, f) \rfloor;$$
$$COH_{p_i p_j}(\Delta y, f) = \left| S_{p_i p_j}(\Delta y, f) \right| \Big/ \left(S_{p_i}(\Delta y, f) S_{p_j}(\Delta y, f) \right)^{1/2} \tag{15}$$

where $COH_p(\Delta y, f)$: N-by-M spanwise coherence matrix; Δy : spanwise separation; $S_{p_i}(\Delta y, f)$, $S_{p_j}(\Delta y, f)$, $S_{p_i p_j}(\Delta y, f)$: auto power spectra of $p_i(y,t)$, $p_j(y+\Delta y,t)$ and cross power spectrum between $p_i(y,t)$ and $p_j(y+\Delta y,t)$; N, and M: numbers of investigated chordwise positions and of spanwise separations. It is noted that the spanwise coherence matrix is a frequency-dependant positive-definite rectangular one, in which their values vary between 0 and 1 at any frequency.

Space functions can be determined based on the singular value decomposition of the spanwise coherence matrix of the fluctuating pressure fields

$$COH_p(\Delta y, f)\Omega_1(\Delta y, f) = \mathrm{E}(f)\Omega_2(\Delta y, f) \tag{16}$$

where $\mathrm{E}(f)$: coherence singular value matrix $\mathrm{E} = diag[\varepsilon_1(f), \varepsilon_2(f), \ldots \varepsilon_K(f)]_{NxM}$; and $\Omega_1(\Delta y, f)_{MxM}, \Omega_2(\Delta y, f)_{NxN}$: coherence space functions containing frequency-dependant singular vectors (or coherence POD modes) orthogonalized at each frequency. Noting that the coherence singular values are positive real, the coherence shape functions are also positive-definite real square matrices.

The spanwise coherence matrix of the fluctuating pressure field can be approximated using a limited number of low-order coherence POD modes

$$COH_p(\Delta y, f) = \Omega_2(\Delta y, f)\mathrm{E}(f)\Omega_1(\Delta y, f)^{*T} \approx \sum_{i=1}^{\tilde{N}} \omega_{2i}(\Delta y, f)\varepsilon_i(f)\omega_{1i}(\Delta y, f)^{*T}, \quad \tilde{N} < N \tag{17}$$

The importance of the coherence POD modes can be evaluated using a similar concept of energy contribution. The energy contribution of the i-th coherence mode on total field energy can be determined by Eq.(14). Because of their contributive energy proportions, the lowest coherence POD modes can be used to investigate the spanwise coherence of the unsteady pressure field.

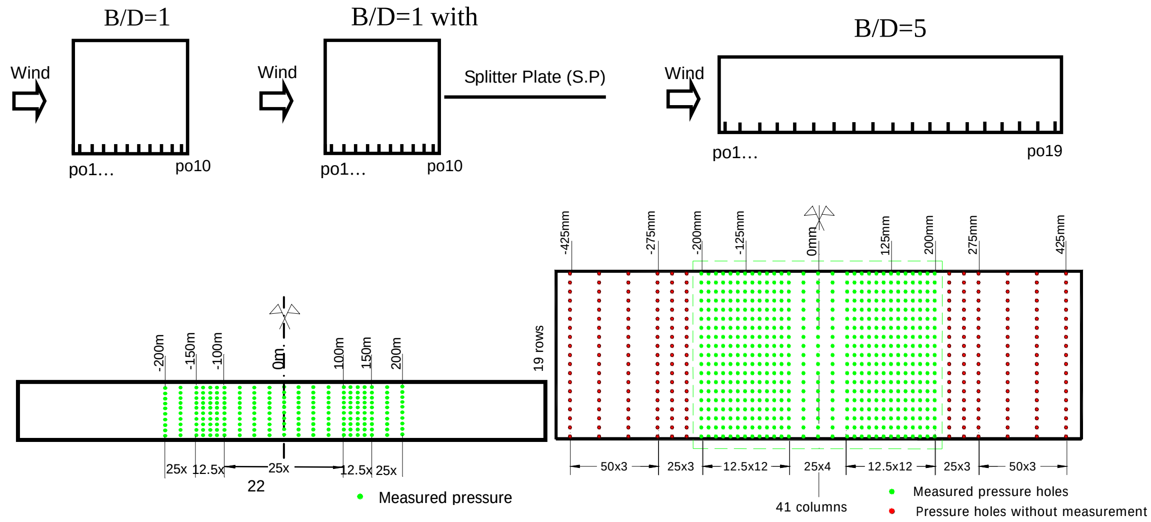

(a) B/D=1 (b) B/D=1 with Splitter Plate (c) B/D=5

Fig. 1 Experimental models and pressure tape arrangement

3. Unsteady pressure measurements on prisms

Physical measurements of unsteady pressures have been carried out on three motionless models with typical slenderness ratios B/D=1, B/D=1 with splitter plate (S.P) in wake of the model and B/D=5 (B, D: width and height of models). Grid turbulent flows were generated in the wind tunnel.

Two u-, w-turbulence components were measured by x-type hot-wire anemometers in spatial positions in wind tunnels without the models for three turbulent flow cases corresponding to turbulence intensities I_u=11.46%, I_w=11.23% (flow case 1), I_u=10.54%, I_w=9.28% (flow case 2) and I_u=9.52%, I_w=6.65% (flow case 3). Because this study focuses on the pressure field itself and symmetrical, montionless models are used, thus pressure taps were only arranged inside the models and on the lower surfaces of the models in chordwise and spanwise positions. There were 10 chordwise pressure taps in models B/D=1 and 19 chordwise pressure taps in model B/D=5 (see Fig. 1). Moreover, the pressure taps were installed at various spanwise separations for investigating spanwise correlation and coherence, as well as convective flow. Unsteady pressures were simultaneously measured by a multi-channel pressure measurement system (ZOC23). All electric signals were filtered by 100 Hz low-pass filters before passing through an A/D converter at a sampling rate of 1000 Hz for 100 seconds. Selected sampling rate and duration of the measured pressures would be satisfactory for expected real and bin frequency resolutions in order to identify and separate spectral components and physical events inside the unsteady pressures. Concretely real frequency resolution here can be analyzed and separated at 0.01 Hz.

Bluff body flow was assumed around the models due to interaction between ongoing turbulent flow and a motionless model. Bluff body flow characterizes not only chordwise flow behaviors at leading edge, trailing edge, on surface and wake of the model such as formatting separated and reattached flows, separation bubble and vortex shedding, but also convective flow in the spanwise direction. It can be predicted from previous studies that model B/D=1 is favorable for formation of Karman vortex shedding at the wake, whereas model B/D=5 is typical for formatting separated and reattached flows on the surface and a separation bubble in the leading edge region as well. The splitter plate was added to model B/D=1 in order to suppress the effect of the Karman vortex in the wake.

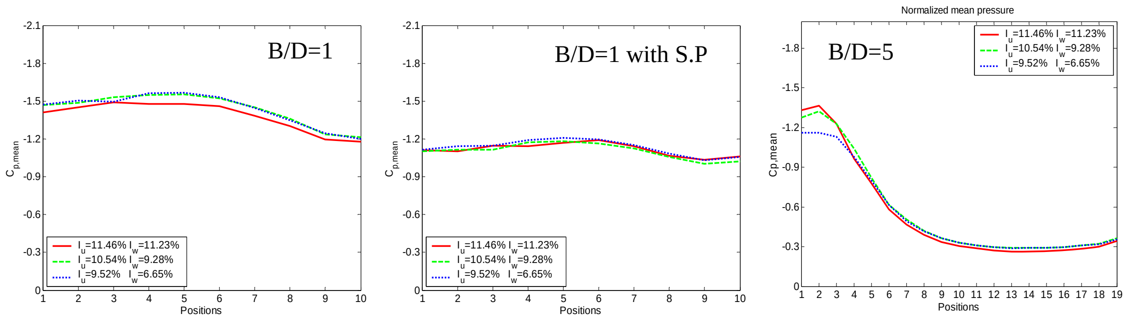

(a) Normalized mean pressure

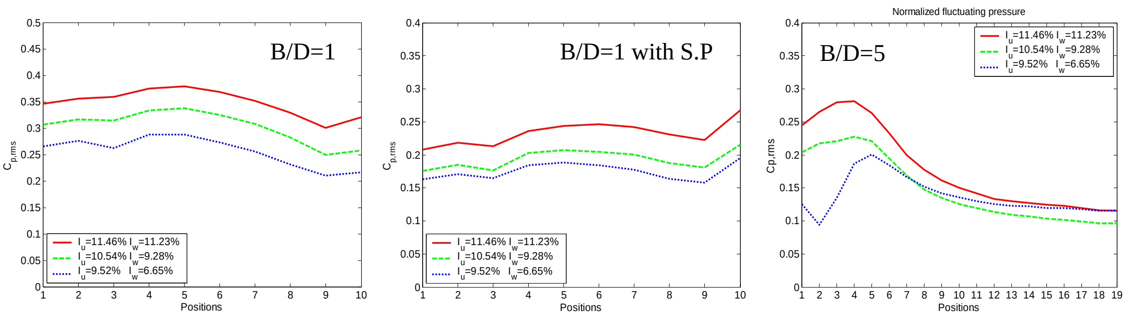

(b) Normalized fluctuating pressure

Fig. 2 Normalized mean and fluctuating pressure distributions on chordwise positions for three flow cases

4. Chordwise pressure distribution and bluff body flow pattern

Fig. 2 shows the chordwise distribution of normalized mean pressures and of normalized fluctuating pressures on the three models in three turbulent flows. As can be seen, the fluctuating pressure is distributed uniformly on the surface of models B/D=1 whereas it is distributed dominantly in the leading edge region of model B/D=5. The fluctuating pressures, furthermore, decrease with decrease in turbulence intensities.

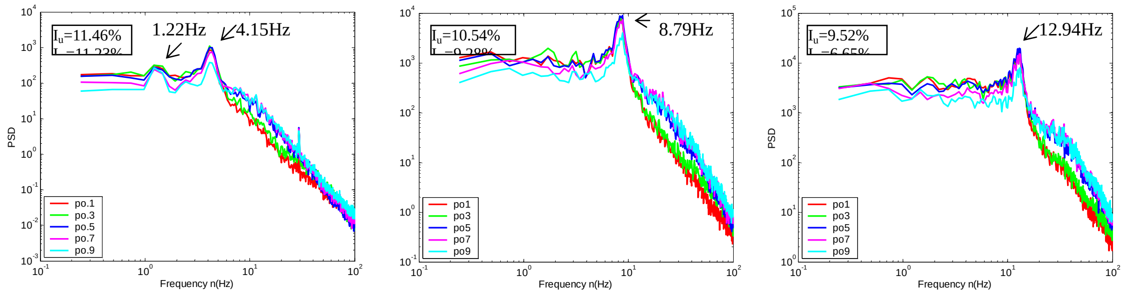

(a) B/D=1

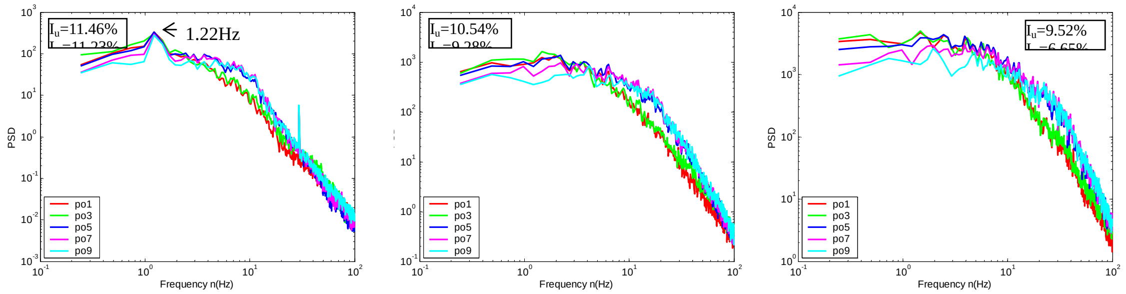

(b)B/D=1 with S.P

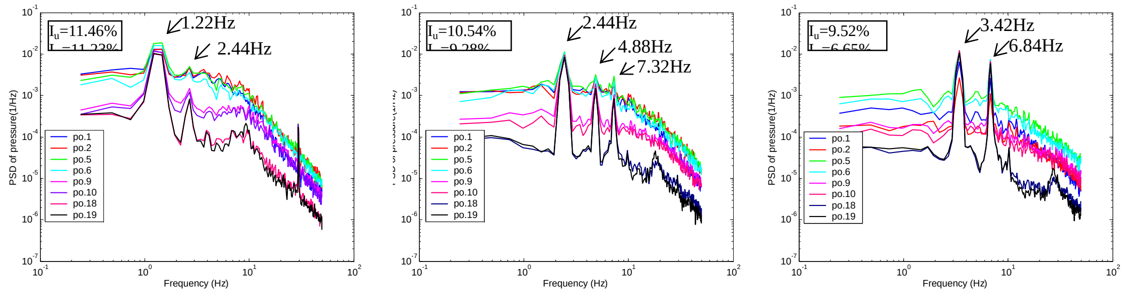

(c) B/D=5

Fig. 3 Power spectra of fluctuating pressures in chordwise positions for three flow cases

The power spectra of fluctuating pressures at some chordwise positions for three models and three mean wind velocities are shown in Fig. 3. For model B/D=1, peak frequencies are observed at 4.15 Hz, 8.79 Hz and 12.94 Hz for the three turbulent flows. It is explained that a Karman vortex formed and shed at the wake of the model. Shedding frequency depends on the Strouhal number (S_t) of the square prism. Moreover, the Strouhal number can be determined as S_t=0.1285.

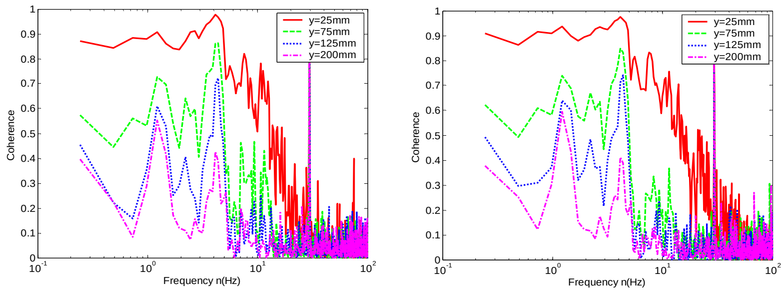

(a) B/D=1

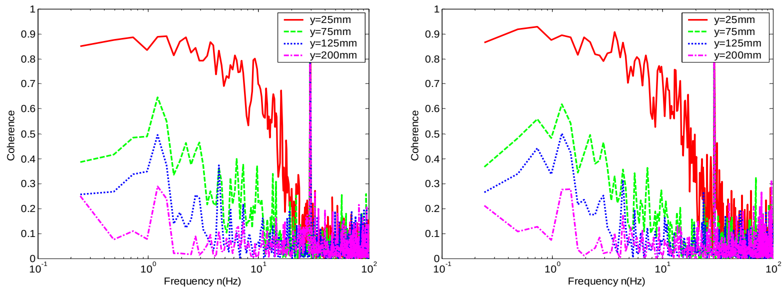

(b) B/D=1 with S.P

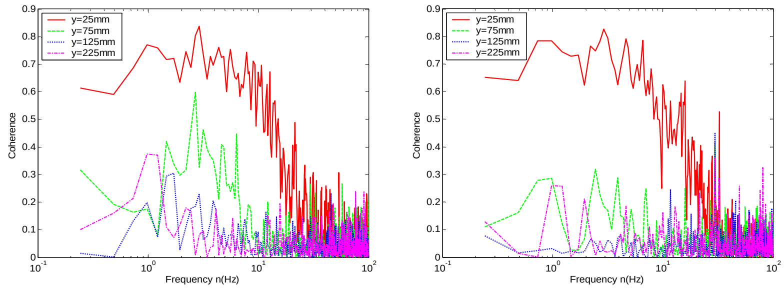

(c) B/D=5

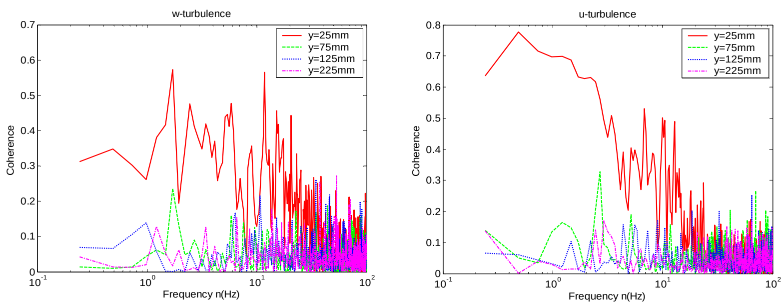

(d) w-turbulence (e) u-turbulence

Fig. 4 Effect of spanwise separation on spanwise coherence of pressure and turbulence (flow case 1)

For B/D=1 with a splitter plate, no peak frequency is observed. This also means that no Karman vortex occurred and the splitter plate suppressed the Karman vortex. Spectral peaks are also observed at frequencies 1.22 Hz and 2.44 Hz; at 2.44 Hz, 4.88 Hz, 7.32 Hz; at 3.42 Hz and 6.84 Hz in the three flow cases. It is predicted that the bluff body flow is separated and reattached on the model surface. Reattachment points for the bluff body flow are determined roughly at positions 6, 7, and 8 with respect to an increase in mean wind velocities. It is assumed that the observed spectral peaks are induced by rolled-up vortices shed at the reattachment points toward the trailing edge. This agrees with findings presented by Hiller and Cherry, 1981, in which empirical formulae were proposed to estimate frequency of rolled-up vortices shedding at the reattachment point depending on mean velocity and length of separation bubble.

5. Spanwise pressure coherence

Spanwise coherence of the unsteady pressure fields on the three prisms has been investigated with effects of spanwise separations, chordwise pressure positions and Karman vortex. Fig. 4 shows the effect of spanwise separations ($\Delta y = 25, 75, 125, 225mm$) on the coherences of pressure and u-, w-turbulences for the three prisms and in the frequency band 0÷100 Hz (for only flow case 1 discussed here). Spanwise coherence reduces considerably with an increase in the spanwise separation and observed frequency. Coherences of pressures and turbulences are significant at close separations and in low-frequency bands. The pressure coherence shows sudden rises at distant separations and at certain frequencies. This might be explained by physical events occurring on the prism surface, such as Karman vortex shedding in the wake and rolled-up vortex shedding at the reattachment point. Fig. 5 shows the pressure coherences at chordwise positions 1, 3, 5, 7, 9 (models B/D=1 without and with S.P) and positions 1, 4, 8, 19 (model B/D=5) and at spanwise separations $\Delta y = 25$ and 75 mm. As shown, the spanwise coherence depends on the chordwise pressure positions. This is assumed to be due to behavior of the bluff body flow in the chordwise direction. It can be seen from Figure 5 that the pressure coherences on models B/D=1 seem to be similar, except at the vortex shedding frequencies, whereas a difference in pressure coherence on model B/D=5 is observed. For model B/D=5, the pressure coherence at position 1 (at the leading edge) seems to be large for close separation Δy =25 mm and small for distant separations Δy =75,125 mm; large for all separations at position 4 (in the separation bubble); small for all separations at position 8 (at the attachment point); and small for close separation Δy =25 mm and strong for distant separations Δy =75 mm at position 19 (at the trailing edge) (see Fig. 5(c)). Therefore, it might be assumed that the pressure coherence is relatively high in the separation bubble region, and to be relatively small in the reattachment region. The effect of pressure positions and bluff body flow must be involved in the higher mechanism of pressure coherence. Fig. 6 compares the pressure coherences at two referred pressure positions 3 and 7, on the three prisms and that of u-, w-turbulences. Obviously, the pressure coherences are larger than the turbulence coherences at the same separations. Moreover, the pressure coherences on the three models decrease for models B/D=1 and B/D=1 with S.P to B/D=5. Clearly, the pressure coherence in the presence of the Karman vortex is larger than that without the Karman vortex. In other words, the Karman vortex also enhances the spanwise convection of the bluff body flow. It can be generalized that the pressure coherence decreases with increase in the spanwise separation, frequency, slenderness ratio and modified geometrical parameters such as the splitter plate in the flow wake, cutting-sharp corners at the trailing edge and so on.

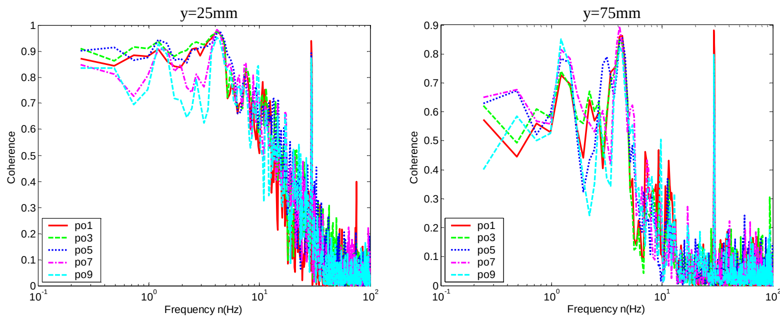

(a) B/D=1

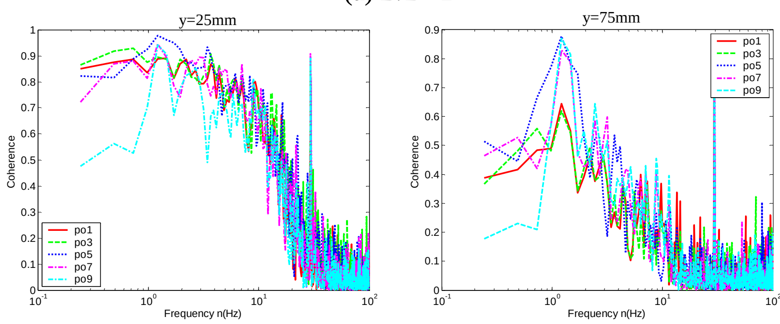

(b) B/D=1 S.P

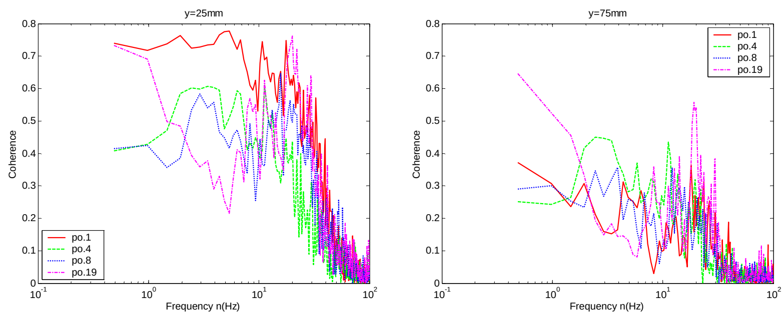

(c) B/D=5

Fig. 5 Effect of chordwise pressure position on spanwise coherence (flow case 1)

6. Analysis and synthesis of unsteady pressure fields

6.1 Analysis and synthesis on covariance proper orthogonal decomposition

Covariance eigenvalues and covariance POD modes have been determined from the eigenvalue decomposition of the covariance matrices of chordwise fluctuating pressure fields on the three prisms. Fig. 7 shows the first four covariance POD modes along chordwise positions for flow case

1 (two other flow cases not being interpreted here for a sake of brevity). It is observed that the first covariance POD modes of all three prisms look like the fluctuating pressure distributions in the chordwise direction.

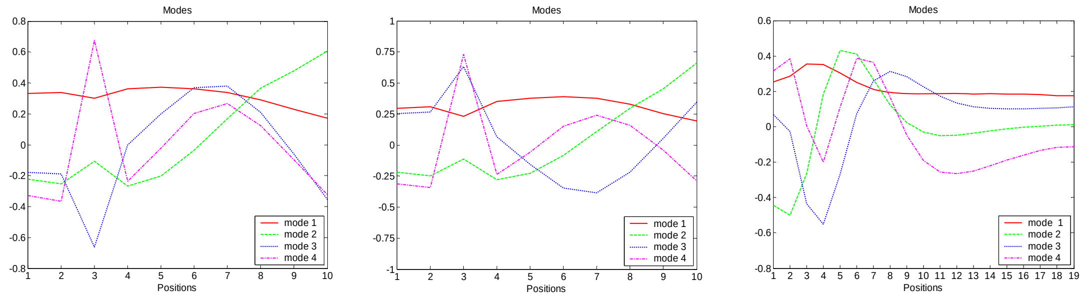

(a) B/D=1 (b) B/D=1 with S.P (c) B/D=5

Fig. 7 First four covariance modes (flow case 1)

Table 1 Energy contribution of covariance POD modes (unit: %)

Mode	B/D=1			B/D=1 with S.P			B/D=5		
	3 m/s	6 m/s	9 m/s	3 m/s	6 m/s	9 m/s	3 m/s	6 m/s	9 m/s
1	76.92	77.46	75.36	65.29	62.79	63.30	43.77	44.86	65.9
2	13.27	13.25	14.41	20.97	22.61	22.08	22.02	23.14	13.29
3	4.69	4.23	4.62	6.14	6.29	6.10	15.18	15.14	9.48
4	2.87	2.86	3.17	4.04	4.32	4.41	5.98	5.68	3.4
5	1.27	1.32	1.45	1.99	2.28	2.45	4.76	4.11	2.79

The energy contribution of the lowest five modes is given in Table 1, and is estimated from Eq. (9). The first covariance POD mode contributes dominantly to all pressure fields. The first modes contribute 76.92%, 65.29%, and 43.77% to the total field energies corresponding to models B/D=1, B/D=1 with S.P and B/D=5, respectively. If the first two covariance POD modes are taken in combination, the cumulative energies of these modes holds up to 90.19%, 86.26%, and 65.79% of their field energies. In other words, the first covariance POD modes contribute dominantly, and the combined first two modes contribute almost all the pressure field energy. It is also noted that the first covariance POD mode for model B/D=5 contributes much lower energy in comparison with models B/D=1. It is assumed that the complexity of the bluff body flow on model B/D=5 reduces the role of the first covariance POD mode.

Uncorrelated principal coordinates associated with the covariance POD modes have been determined from the measured data as the first four principal coordinates of the three models and their corresponding power spectra and are shown in Fig. 8. It is noteworthy that the first principal coordinates not only dominate in the power spectrum but also contain frequency characteristics of their pressure fields, whereas the other principal coordinates do not have these characteristic frequencies. Therefore, the first covariance POD modes and their associated principal coordinates play an important role in identifying the unsteady pressure fields due to their dominant energy contribution and frequency containing physical events of these pressure fields.

Effects of basic and cumulative covariance POD modes on the synthesis of the pressure fields and the role of the first covariance POD modes on the field identification have also been investigated. Fig. 9 indicates the pressure reconstruction at referred position 5 using individual covariance POD modes (from the first to the fourth covariance POD modes) and cumulative covariance POD modes (using the first covariance POD mode and combined first two POD modes) with verification of the spectral contribution of the covariance POD modes to targeted original pressure. For a brevity, only position 5 and flow case 1 are presented here. As can be seen from Fig. 9, the synthesis of the fluctuating pressures using the first covariance POD mode is similar to the original pressures. Reconstructed pressures containing the frequency peaks can be used to identify hidden events and physical phenomena of the original pressure fields. In comparison, reconstructed pressure portions using the second covariance POD mode, the third mode and the fourth mode show minor contributions to the original pressure. Moreover, these pressure portions do not contain frequency peaks in the targeted original pressure. Reconstructed pressure using the first covariance POD mode, moreover, seems to be in good agreement with the targeted original one in the low-frequency range between 0÷10Hz for models B/D=1, but there is a notable difference between the reconstructed pressure and the original one in the high-frequency range for models B/D=1 and all frequency ranges (except at the frequency peaks) for model B/D=5. It is assumed that the first covariance POD mode is enough for synthesis of the pressure fields at low frequencies for models B/D=1, but more cumulative POD modes might be needed for the reconstructed pressure at high frequencies. For model B/D=5, moreover, the first covariance POD mode can be used to identify the pressure field, but it is not enough to reconstruct the original pressure fields. Thus, more covariance POD modes are required for the reconstructed pressures due to the more complicate distribution of the pressure field. In Fig. 10, the reconstructed pressures using the first covariance POD modes and cumulative first two modes and their power spectra are presented. It can be seen that only the first covariance POD mode is enough to reconstruct the original pressure for models B/D=1, and the cumulative first two POD modes are enough for model B/D=5.

6.2 Analysis and synthesis on spectral proper orthogonal decomposition

Spectral eigenvalues and spectral POD modes have been obtained via eigenvalue decomposition of the cross spectral matrices of the fluctuating pressure fields on the three prisms. Fig. 10 shows the first five spectral eigenvalues in frequency band 0÷50Hz for the flow case 1. As can be seen, all first spectral eigenvalues obtained from the pressure fields of the three models are much more dominant than the others. In particular, the first spectral eigenvalues also contain all frequency peaks of the pressure fields, whereas the other eigenvalues do not contain these characteristic peaks.

The first three spectral POD modes of the chordwise fluctuating pressure fields of the three experimental models in the flow case 1 are shown in Fig. 11 for frequency band 0÷50Hz. Information of space and frequency can be observed in these spectral POD modes. However, a linkage between the spectral POD modes and the physical causes on the prisms is still not clear. More investigations should be required for the physical interpretation of experimental spectral POD modes.

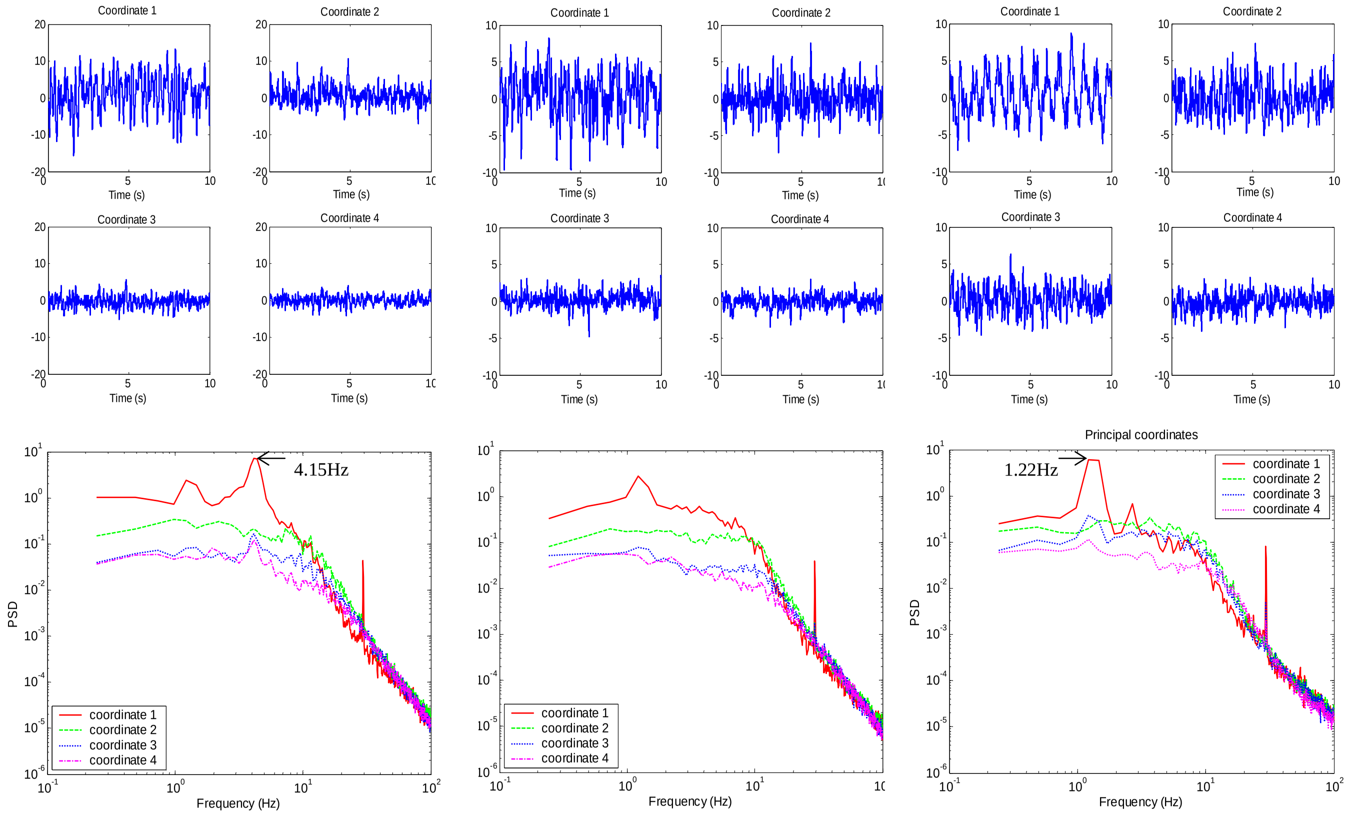

(a) B/D=1 (b) B/D=1 with S.P (c) B/D=5

Fig. 8 First four covariance principal coordinates and their power spectra densities (flow case 1)

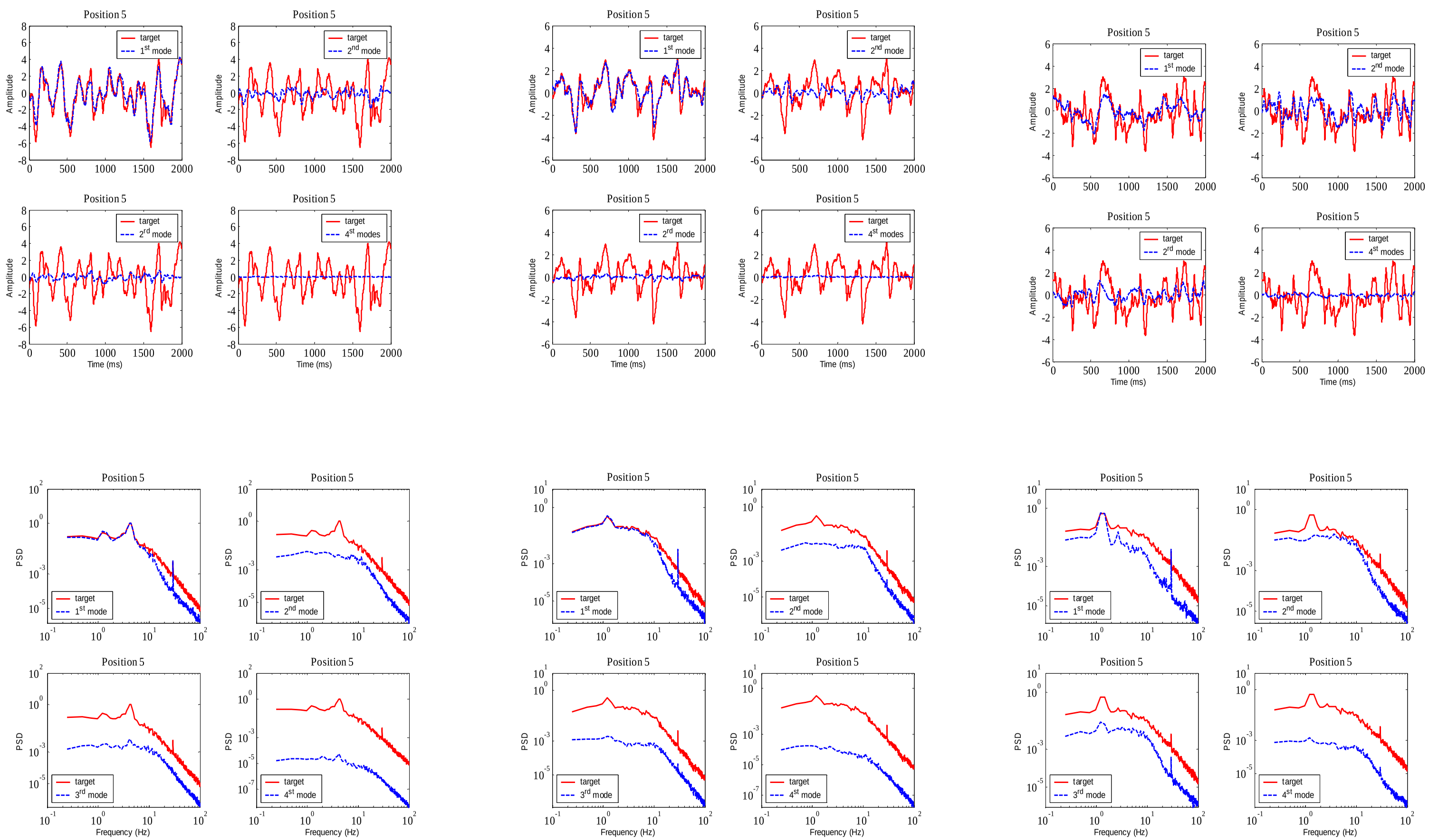

(a) B/D=1 (b) B/D=1 with S.P (c) B/D=5

Fig. 9 Effect of cumulative spectral modes on pressure synthesis at referred position 5 (flow case 1)

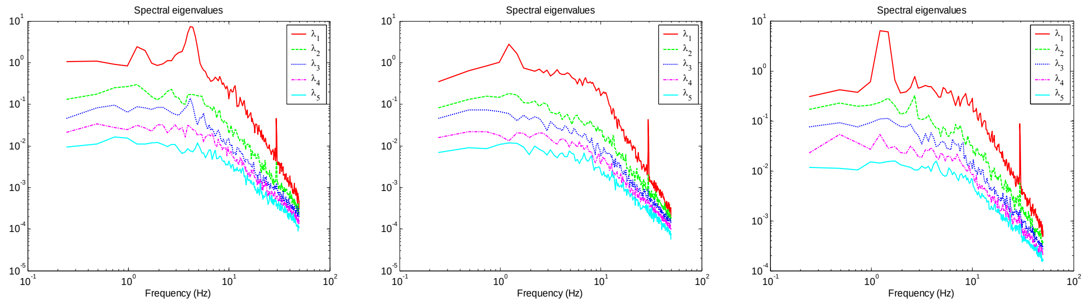

(a)B/D=1 (b) B/D=1 with S.P (c) B/D=5

Fig. 10 First five spectral eigenvalues (flow case 1)

Energy contributions of the spectral POD modes are given in Table 2. Similar to the covariance POD modes, the first spectral POD modes contain dominantly the field energies. The first spectral POD mode contributes 86.04%, 81.30%, and 74.77%, respectively for the three experimental models for flow case 1. Therefore, the first spectral POD modes dominate in the energy contribution for all three prisms. Moreover, the energy contributions of the first spectral POD modes are higher than those of the first covariance POD modes for all models including model B/D=5. This suggests that the first spectral POD mode may provide a better solution than the first covariance POD mode because of its higher energy contribution. The first two spectral POD modes hold almost 94.12%, 91.45% and 87.45% of the pressure field energies for the three models. In other words, the first two spectral POD modes contribute almost all the pressure field energies in these investigated cases.

Table 2 Energy contribution of spectral POD modes (unit: %)

Mode	B/D=1			B/D=1 with S.P			B/D=5		
	3 m/s	6 m/s	9 m/s	3 m/s	6 m/s	9 m/s	3 m/s	6 m/s	9 m/s
1	86.04	85.84	83.02	81.30	77.48	77.88	74.77	73.59	83.93
2	8.08	8.08	9.92	10.15	12.36	11.98	12.68	14.03	7.69
3	3.28	3.20	3.68	4.44	5.14	5.00	5.68	5.56	3.57
4	1.40	1.62	1.94	2.05	2.63	2.70	2.75	2.86	1.86
5	0.64	0.72	0.81	1.09	1.28	1.34	1.44	1.45	1.06

Fig. 12 shows the effects of individual and cumulative spectral POD modes on the synthesis of auto power spectra of the fluctuating pressures. Here, only pressure at position 5 is used for discussion. As can be seen in Figure 12, the first spectral POD mode exhibits sufficient accuracy to reconstruct and identify the original pressure in all three experimental models and all frequency ranges. There are also good agreements between the power spectra of the original pressures and those of the reconstructed pressures for the first spectral POD mode and the first two spectral POD modes.

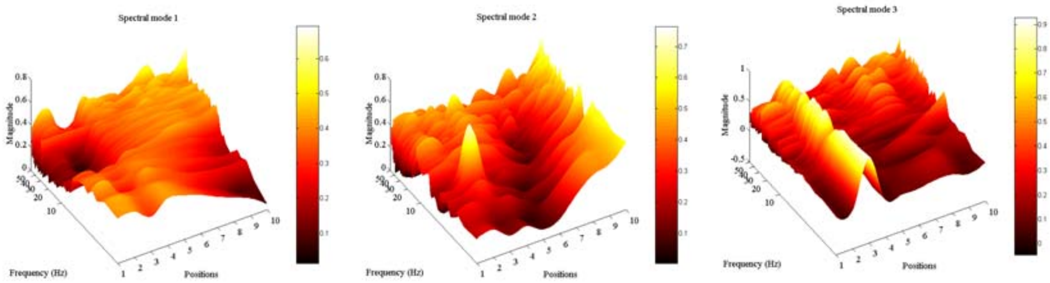

(a) B/D=1

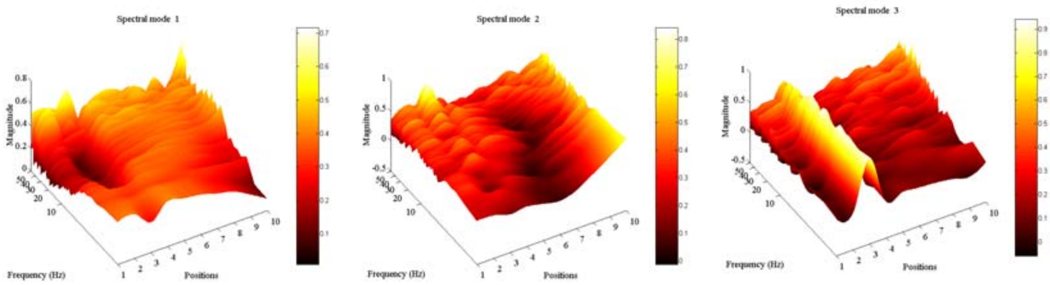

(b) B/D=1 with S.P

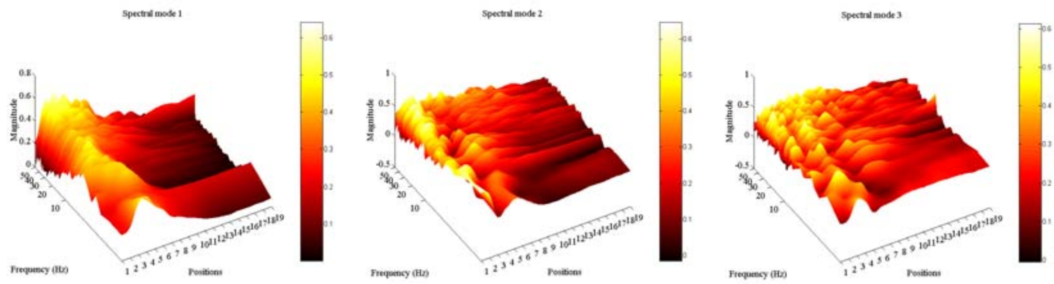

(c) B/D=5

Fig. 11 First three spectral modes

7. Mapping of spanwise pressure coherence

Spanwise coherence matrices of fluctuating pressure fields on the three models B/D=1, B/D=1 with S.P and B/D=5 for the flow case 1 have been constructed before singular value decomposition to determine the coherence singular values and the coherence POD modes. The energy contribution of the first coherence POD modes of the three models can be estimated as 56%, 55%, and 50%, respectively, in the computed frequency range 0÷100Hz based on their associated singular values. If the low-frequency range of 0÷10Hz is taken into account, the first coherence POD modes of models B/D=1, B/D=1 with S.P and B/D=5 contribute up to 89%, 82% and 73% of the total energy of the three pressure fields.

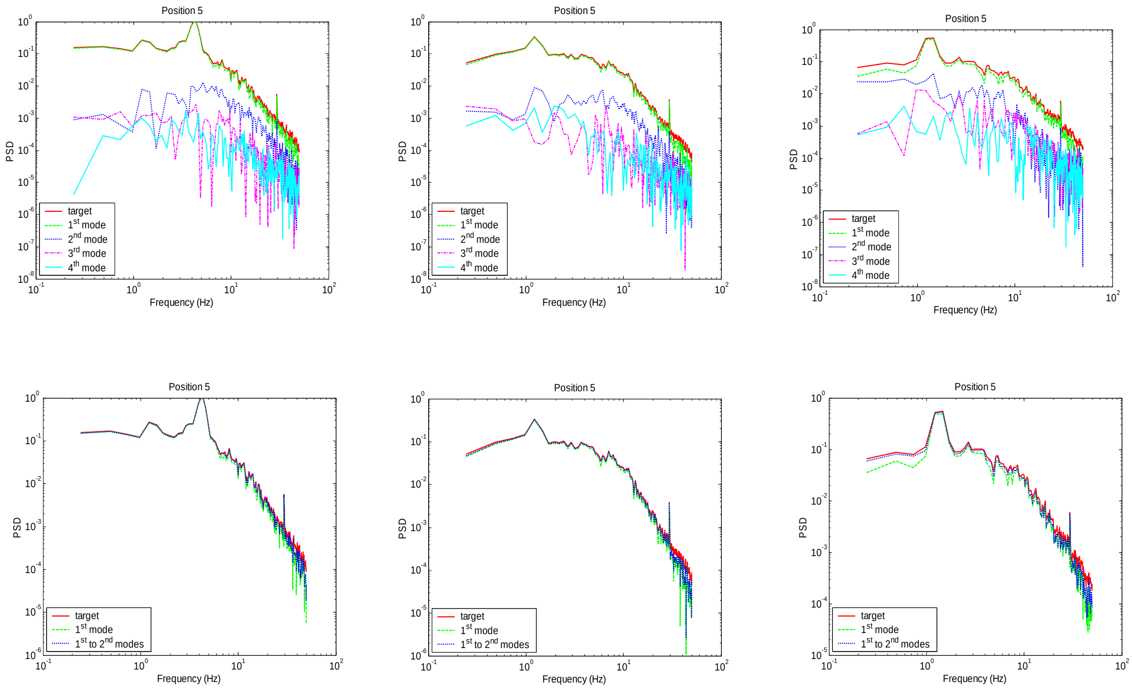

(a) B/D=1 (b) B/D=1 with S.P (c) B/D=5

Fig. 12 Effects of basic and cumulative spectral modes on auto spectral pressure synthesis at referred position 5 (flow case 1)

Fig. 13 shows the first coherence POD modes of the pressure fields for the three models B/D=1, B/D=1 with S.P and B/D=5 with respect to the effect of spanwise separation and of chordwise pressure position (or the bluff body flows). Apparently, the pressure coherence considerately reduces with increase in the spanwise separation and the observed frequency. Moreover, the effects of bluff body flow and chordwise position can also be observed in Fig. 13. Interestingly, highly spanwise coherence and strongly convective bluff body flow might occur locally in the leading edge region and in the separation bubble of model B/D=5, whereas the spanwise coherence seems to uniformly distributed over all chordwise positions of the models B/D=1 and B/D=1 with S.P. These findings are similar to the results for the spanwise coherence presented in the previous parts. However, the first coherence POD modes here are more meaningful because they contain a lot of information on the spanwise separation, observed frequencies and chordwise positions as well.

Thus, they can be used to map intrinsic characteristics of the spanwise coherence of unsteady pressure fields.

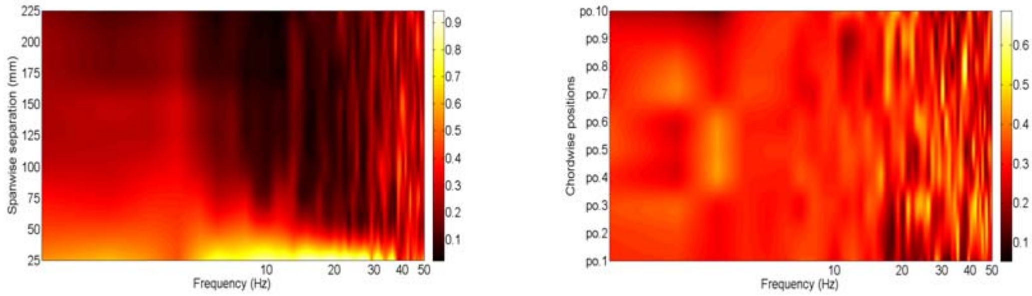

(a)B/D=1

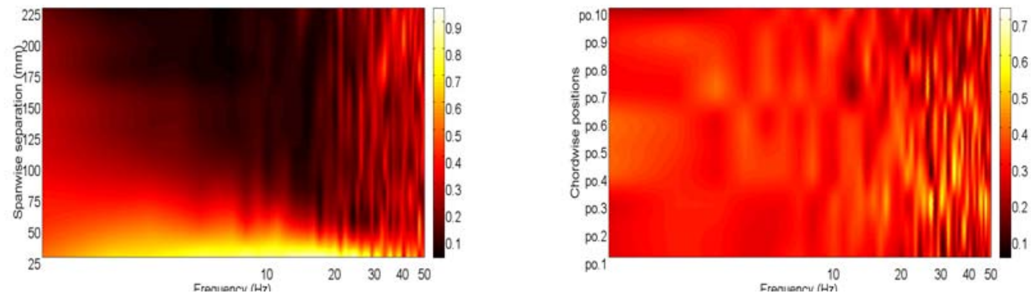

(b) B/D=1with S.P

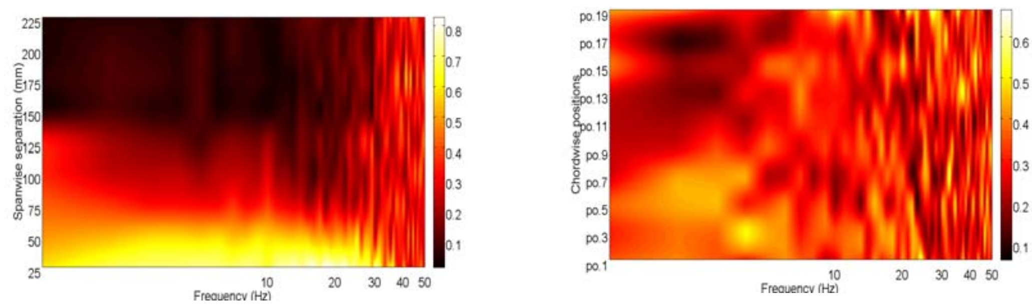

(c) B/D=5

Fig. 13 First two coherence POD modes for mapping pressure coherences (flow case 1)

8. Conclusions

Chordwise distribution and spanwise correlation of the unsteady pressure fields on some typical prisms have been investigated based on both the covariance and spectral proper orthogonal decompositions. Coherence maps of the spanwise pressure fields also have been built the first time ever using the spectral proper orthogonal decomposition.

Analysis and synthesis of the fluctuating chordwise pressures have been carried out. Moreover, intrinsic characteristics of these pressure fields can be identified via low-order POD modes, eigenvalues and principal coordinates. The importance of the first POD mode and its associated quantities has been verified for analysis and synthesis of the unsteady pressure fields. The first covariance principal coordinate and the first spectral eigenvalue contain the characteristic frequency peaks of intrinsic physical events for the unsteady pressure fields. Due to it's the dominant contribution to the pressure field energy, only the first POD mode is accurate enough to reconstruct the pressure field, especially in the low-frequency range. However, more POD modes are required to reconstruct the pressure field in the high-frequency range and for complicated pressure distributions. In comparison, the first spectral POD mode expresses the better solution than the first covariance POD mode for reconstructing the pressure fields.

Linkage between the low-order POD modes and the intrinsic physical events has been validated in investigated cases due to the dominant energy contribution of the lowest-order POD modes and the simple behavior of the pressure fields on the typical prisms. Because the POD modes, eigenvalues and principal coordinates in both the covariance and spectral proper orthogonal decompositions can sensitively depend on the parameters of the experimental pressure fields such as the number of pressure positions, the pressure arrangements, the turbulent flows, the bluff body flow and so on, in such cases of the low-energy contribution, the linkage between the lowest-order POD modes and the physical events cannot be clearly observed. However, more investigations are required to clarify this argument.

Spanwise coherence of the pressure fields has been clarified via the coherence POD mode. Obviously, the effects of spanwise separations, frequencies, and bluff body flows have been observed through the first coherence POD mode. Thus, this POD mode can be used to map the intrinsic characteristics for the spanwise coherence of the unsteady pressure fields.

Acknowledgements

This study was partially funded by the Ministry of Education, Culture, Sport, Science and Technology (MEXT), Japan through the Global Center of Excellence (Global COE) Program, 2008-2012.

References

Berkooz, G., Holmes, P. and Lumley, J.L. (1993), "The proper orthogonal decomposition in the analysis of turbulent flows, *Annu. Rev. Fluid Mech.*, **25**, 539-575.

Bienkiewicz, B., Tamura,Y., Ham, H.J., Ueda, H. and Hibi, K. (1995), "Proper orthogonal decomposition and construction of multi-channel roof pressure", *J. Wind Eng. Ind. Aerod.*, **54-55**, 369-381.

Carassale, L., Solari, G. and Tubino, F. (2007), "Proper orthogonal decomposition in wind engineering. Part 2: Theoretical aspects and some application", *Wind Struct.*, **10**(2), 177-208.

Davenport, A.G. (1963), "The response of slender, line-like structures to a gusty wind", *Proc. Inst. Civil Engineers*, **23**, 389-408.

De Grenet, E.T. and Ricciardelli, F. (2004), "Spectral proper transformation of wind pressure fluctuation: application to a square cylinder and a bridge deck", *J. Wind Eng. Ind. Aerod.*, **92**, 1281-1297.

Hillier, R. and Cherry, N.J. (1981), "The effects of stream turbulence on separation bubbles", *J. Wind Eng. Ind. Aerod.*, **8**, 49-58.

Holmes, J.D., Sankaran, R., Kwok, K.C.S. and Syme, M.J. (1997), "Eigenvector modes of fluctuating pressures on low-rise building models", *J. Wind Eng Ind. Aerod.*, **69-71**, 697-707.

Jakobsen, J.B. (1997), "Span-wise structure of lift and overturning moment on a motionless bridge girder", *J. Wind Eng. Ind. Aerod.*, **69-71**, 795-805.

Jeong, S.H., Bienkiewicz, B. and Ham, H.J. (2000), "Proper orthogonal decomposition of building wind pressure specified at non-uniform distributed pressure taps", *J. Wind Eng.Ind. Aerod.*, **87**, 1-14.

Kareem, A. (1997), "Correlation structure of random pressure fields", *J. Wind Eng. Ind. Aerod.*, **69-71**, 507-516.

Kikuchi, H., Tamura, Y., Ueda, H. and Hibi, K. (1997), "Dynamic wind pressure acting on a tall building model - Proper orthogonal decomposition", *J. Wind Eng. Ind. Aerod.*, **69-71**, 631-646.

Kimura, K., Fujino, Y., Nakato, S. and Tamura, H. (1997), "Characteristics of buffeting forces on plat cylinders", *J. Wind Eng. Ind. Aerod.*, **69-71**, 365-374

Larose, G.L. (1996), "The span-wise coherence of wind forces on streamlined bridge decks", *Proceedings of the 3rd Int'l Colloquium on Bluff Body Aerodynamics and Applications*, Blacksburg, USA.

Le, T.H, Matsumoto, M. and Shirato, H. (2009), "Spanwise coherent structure of wind turbulence and induced pressure on rectangular cylinders", *Wind Struct.*, **12**(5), 441-455.

Le, T.H, Tamura, Y. and Matsumoto, M. (2011), "Spanwise pressure coherence on prisms using wavelet transform and spectral proper orthogonal decomposition based tools", *J. Wind Eng. Ind. Aerod.*, **99**, 499-508.

Liang, Y.C., Lee, P., Lim, W.Z., Lee, K. and Wu, C.G. (2002), "Proper orthogonal decomposition and its applications – Part I: Theory', *J. Sound Vib.*, **252**(3), 527-544.

Lumley, J.L. (1970), *Stochastic tools in turbulence*, Academic Press.

Matsumoto, M., Shirato, H., Araki, K., Haramura, T. and Hashimoto, T. (2003), "Spanwise coherence characteristics of surface pressure field on 2-D bluff bodies", *J. Wind Eng. Ind. Aerod.*, **91**,155-163.

Solari, G., Carassale, L. and Tubino, F. (2007), "Proper orthogonal decomposition in wind engineering. Part 1: A state-of-the-art and some aspects", *Wind Struct.*, **10**(2), 153-176.

Tamura, Y., Ueda, H., Kikuchi, H., Hibi, K., Suganuma, S. and Bienkiewicz, B. (1997), "Proper orthogonal decomposition study of approach wind-building pressure correlation", *J. Wind Eng. Ind. Aerod.*, **72**, 421-431.

Tamura, Y., Suganuma, S., Kikuchi, H. and Hibi, K. (1999), "Proper orthogonal decomposition of random wind pressure field", *J. Fluid. Struct.*, **13**(7-8), 1069-1095.

CC